

Van der Waals spin valves

C. Cardoso, D. Soriano, N. A. García-Martínez, J. Fernández-Rossier ^{*}
QuantaLab, International Iberian Nanotechnology Laboratory (INL),
Av. Mestre José Veiga, 4715-330 Braga, Portugal
 (Dated: February 19, 2024)

We propose spin valves where a 2D non-magnetic conductor is intercalated between two ferromagnetic insulating layers. In this setup, the relative orientation of the magnetizations of the insulating layers can have a strong impact on the in-plane conductivity of the 2D conductor. We first show this for a graphene bilayer, described with a tight-binding model, placed between two ferromagnetic insulators. In the anti-parallel configuration, a band gap opens at the Dirac point, whereas in the parallel configuration, the graphene bilayer remains conducting. We then compute the electronic structure of graphene bilayer placed between two monolayers of the ferromagnetic insulator CrI_3 , using density functional theory. Consistent with the model, we find that a gap opens at the Dirac point only in the antiparallel configuration.

PACS numbers:

The controlled fabrication of layered structures combining ferromagnetic conductors and non magnetic materials, thin enough as to preserve spin polarization, made possible the discovery of fundamental spin dependent transport phenomena, such as Giant Magnetoresistance [1, 2] and tunnel Magnetoresistance [3, 4]. These developments led to the concept of spin valve, a structure whose conductivity is modulated by the relative orientation of two ferromagnetic electrodes [5] and, altogether, set the foundations of spintronics.

The study of the so called Van der Waals heterostructures [6, 7], metamaterials obtained by vertical stacking of 2D crystals, is a very fertile area of research. Using relatively simple fabrication methods, they allow the study of structures with tailored electronic properties that combine a variety of 2D materials, including insulators (h-BN), semiconductors (MoS_2), conductors (graphene) and superconductors (NbSe_2). The recent discovery of 2D crystals with magnetic order [8–11] adds both ferromagnetic and antiferromagnetic insulators to this list. For instance, Van der Waals devices incorporating atomically thin layers of the ferromagnetic insulator CrI_3 , have been reported [12–17]. These findings pave the way to Van der Waals spintronics with new types of spin dependent transport phenomena.

Here we propose a new class of spin valve that takes advantage of the spin proximity effect, *i.e.*, the spin polarization of the surface electrons of a non-magnetic material adjacent to a ferromagnet. The proposed system, depicted in Figure 1, consists of a 2D conducting crystal sandwiched between two insulating ferromagnetic layers. If the magnetizations of the two proximity layers are anti-parallel (AF), the spin proximity effects have opposite sign at both sides of the 2D crystal. In contrast, for the

parallel state (FM), the top and bottom proximity effects add up. As we show below, this difference has a strong influence in the in-plane conductance of the non-magnetic conductor, and in some instances leads to a *conductor to insulator transition* in the 2D crystal. This strong influence of spin proximity effect in a 2D crystals contrast with the case of 3D materials, for proximity effects are constrained to their surface.

Our proposal is different from lateral graphene spin valves [18, 19], where large areas of the graphene are not in contact with ferromagnetic electrodes, and is also different from spin-filter tunnel junctions, where the magnetic insulators act as barrier materials for vertical transport [12–14, 20]. The proposed spin valve resembles the early current in plane structures where giant magnetoresistance was discovered [1, 2], with the obvious difference that the magnetic layers are insulating in the Van der Waals spin valves.

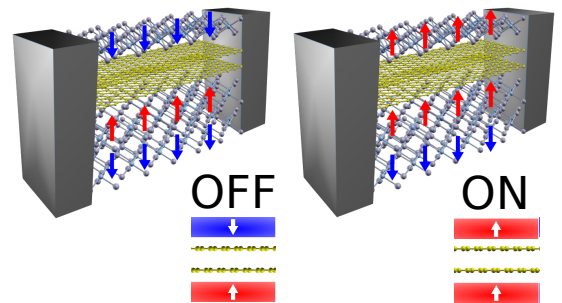


FIG. 1: Van der Waals spin valve, where a conducting 2D crystal is sandwiched between 2 insulating ferromagnets. Lateral contacts can drive in-plane current. The magnetization of the bottom ferromagnetic layer is pinned, whereas the top layer can switch, resulting in two configurations, (a) antiparallel (AF) and (b) parallel (FM), with very different in-plane conductance.

^{*}On leave from Departamento de Física Aplicada, Universidad de Alicante, Spain

We first illustrate the concept of Van der Waals (VdW) spin valves considering the case when the central con-

ductor is a graphene bilayer. We use the standard tight-binding model for the graphene bilayer[21]. Spin proximity effect is considered[22] by including a spin dependent potential Δ whose sign can be different in the top and bottom graphene layers. Previous density functional theory (DFT) calculations for monolayer graphene deposited on different ferromagnetic insulators, such as EuO[23, 24], EuS [24], YIG [24], justify this model. We assume that the magnetization of both top and bottom layers lie on the same axis. We also assume that the bottom magnetization does not change, resulting in fixed spin-dependent potential $\sigma\Delta$, where σ is the spin projection along the magnetization axis. The top layer spin dependent potential is given by $\eta\sigma\Delta$, where $\eta = \pm 1$ describes the magnetization orientation of the top magnetic layer, relative to the bottom layer. Thus, $\eta = +1$ describes the parallel (FM) orientation and $\eta = -1$ the antiparallel (AF) case.

Represented in the basis A_1, B_1, A_2, B_2 , where A and B correspond to the two triangular sublattices, and the subindices 1 and 2 label the top and bottom layers, respectively, the Bloch Hamiltonian for spin σ states reads:

$$\mathcal{H}_\sigma(\vec{k}) = \begin{pmatrix} \eta\sigma\frac{\Delta}{2} & f(\vec{k}) & 0 & 0 \\ f^*(\vec{k}) & \eta\sigma\frac{\Delta}{2} & \gamma & 0 \\ 0 & \gamma & \sigma\frac{\Delta}{2} & f(\vec{k}) \\ 0 & 0 & f(\vec{k})^* & \sigma\frac{\Delta}{2} \end{pmatrix} \quad (1)$$

where $f(\vec{k}) = t \left(1 + e^{i\vec{k} \cdot \vec{a}_1} + e^{i\vec{k} \cdot \vec{a}_2} \right)$ and γ describe the intralayer and interlayer hopping matrix elements, respectively. The resulting spin resolved energy bands, in the neighbourhood of the Dirac point, are shown in fig. 2 for the two states of the spin valve, $\eta = \pm 1$. For the FM alignment ($\eta = +1$), the graphene bilayer presents spin-split bands, and remains in a conducting state, *i.e.*, with a finite density of states at the Fermi energy. In contrast, for the AF case ($\eta = -1$), a band-gap opens up at the Dirac point. Thus, depending on the relative alignment of the top and bottom insulating ferromagnets, the graphene bilayer spin valve can be either a conductor, for the FM alignment, or a gapped system with depleted conductance, when the Fermi energy is set at the Dirac point. Within this model, both the band-gap in the AF alignment and the spin splitting in the FM alignment are given by Δ .

We now address the origin of the gap opening in graphene bilayer AF alignment of the VdW spin valve. For each spin channel, the Hamiltonian (1) in the AF alignment is identical to the model of graphene bilayer with an off-plane electric field, that is known to open up a gap in the band structure [25, 26]. Interestingly, in the spin-valve, the sign of the effective electric field is opposite for opposite spins, $E_{\text{eff}} \propto \sigma\Delta$. The spin projection of the AF bands over top and bottom layers, shown in Fig. 2, clearly shows the presence of a spin dipole[27]: for a given spin, there is a charge imbalance driven by the

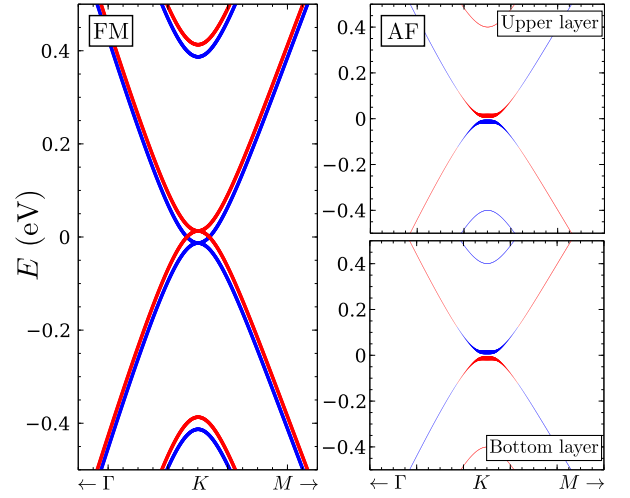


FIG. 2: Bands structure computed with model Hamiltonian for the FM (left) and AF (right) configurations, Red and blue stand for the different spin states. For the AF state, the bands have been projected in the upper and lower layer of the graphene bilayer, with the size of the dots proportional to the layer polarization, revealing that the top of the valence band and bottom of conduction band are spin polarized in each of the layers.

exchange with the magnetic layers, that is compensated exactly by the opposite spin.

In a graphene bilayer, the gap opened by an electric field is known to have a valley dependent Chern number $\mathcal{C} = K \text{sgn}(E)$, where $K = \pm 1$ labels the valleys [28, 29]. In the case of the spin valve in the AF state, this leads to Chern numbers that are both spin and valley dependent:

$$\mathcal{C} = K\sigma = \pm 1 \quad (2)$$

Eq. (2) permits to anticipate [28, 29] the emergence of spin-locked chiral one dimensional in-gap states in domain walls separating two antiferromagnetic domains with opposite magnetizations (see Fig 3). In order to verify this, we compute the momentum resolved density of states of a domain wall along the zigzag direction as illustrated in fig. 3. The domain wall is assumed to be abrupt, preserving spin collinearity. The calculation is done for a system with translational invariance along the wall direction, and embedded between two semi-infinite gapped graphene bilayer planes, using a Green function technique [30]. Both domains are insulating, but at each valley the Chern number is opposite for a given spin direction. Thus, a domain wall along the zigzag direction, that preserves the valley, features two chiral 1D in-gap states per valley and per spin (see fig. 3). It is interesting to note that, for a given valley, the states are spin chiral and therefore back-scattering requires either spin-mixing, or inter-valley scattering. A non collinear domain wall might result in spin mixing.

We now consider a possible physical realization of

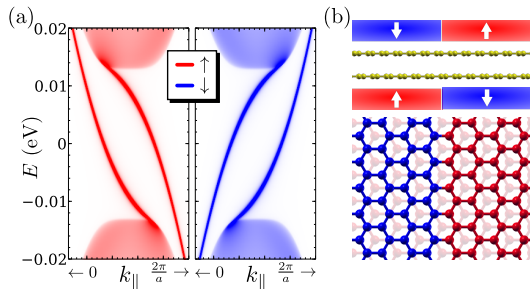


FIG. 3: Chiral in-gap states, for a given valley, computed for the domain wall between two insulating antiferromagnetic domains with opposite spin orientation. The velocity of the bands changes sign in the opposite valley.

the Van der Waals spin valve, based on a graphene bilayer, that is feasible within the experimental state of the art. For that matter, we choose CrI_3 monolayers as the insulating ferromagnet. It was recently shown that CrI_3 monolayers remain ferromagnetic up to 45K [11]. In addition CrI_3 preserves its magnetic properties even when deposited on graphite [11] or encapsulated between graphite electrodes [12–14]. Moreover, the spin proximity effect between CrI_3 and two dimensional WSe_2 has been demonstrated experimentally [31].

The DFT calculations were performed using Quantum ESPRESSO [32] with PBE exchange-correlation potential [33] and PAW pseudopotentials [34, 35] and including van der Waals interactions within the semiempirical method of Grimme (DFT-D2) [36]. Spin orbit interactions, known to be important to determine the magnetic anisotropy of CrI_3 [37], are not included in the calculation, as they are not expected to induce qualitative change in the spin proximity effect discussed here.

We now discuss our results both for monolayer CrI_3 /monolayer graphene as well as graphene bilayer in between two monolayers of CrI_3 . The former permits to rationalize the results of the bilayer. For the bilayer, we use a unit cell with 4 layers, CrI_3 /graphene bilayer/ CrI_3 , and two different geometries: 1) a free standing multilayer and 2) a superlattice with periodic boundary conditions along the off-plane direction. In the case of the superlattice with periodic boundary conditions, we considered the lattice parameter of graphene for the plane and varied the c lattice parameter in order to optimize the interlayer distance by minimizing the total energy. For the free standing multilayer, we used a lattice parameter along z that ensures the absence of interaction between the replicas of the system. In all cases the unit cell contains a 3×3 supercell with 18 carbon atoms per graphene layer, 2 chromium and 6 iodine atoms per CrI_3 layer. Thus, for the sandwiched graphene bilayer, the unit cell has a total of 52 atoms. The calculations show that the spin of Cr atoms is $S = 3/2$, that are hosted by

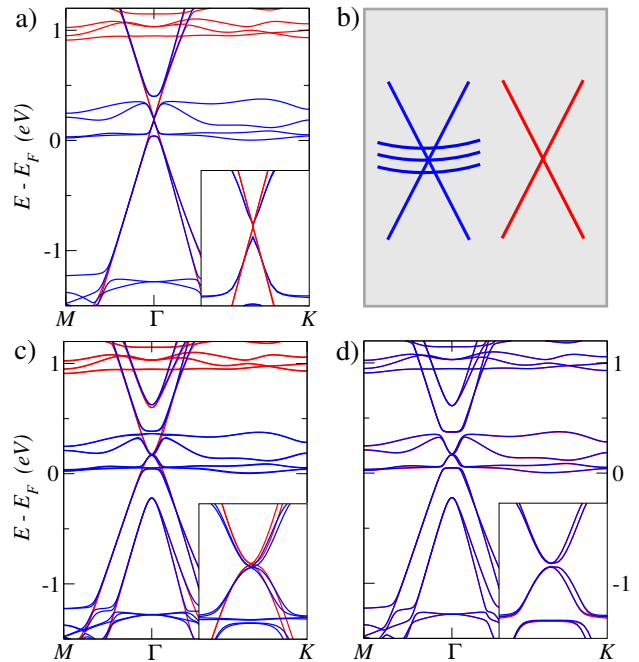


FIG. 4: (a) Band structure, for the graphene monolayer on top of CrI_3 monolayer. (b) Scheme of energy bands for graphene monolayer on CrI_3 . (c) and (d) Band structure for graphene bilayer placed between ferromagnetic monolayers of CrI_3 with FM (c) and AF (d) relative alignment. The insets show a zoom around the Dirac point, showing a spin splitting in the FM alignment and a gap for the AF case, both taking the same value of 7 meV.

the t_{2g} bands.

We first discuss the results for the monolayer graphene on top of CrI_3 , shown in (3)(a). Our results are in line with previous DFT calculations for this system [38]. With the exception of some anti-crossings, the energy bands are an overlay of those of the decoupled monolayers, as expected in a Van der Waals structure. Occupied bands, way below the Fermi energy E_F , are made of iodine p states and the spin majority t_{2g} states of Cr. Empty bands, high above E_F , are made of spin minority t_{2g} states of Cr. In the 2 eV window around the Fermi energy, the bands are those of the graphene Dirac cones and the spin majority e_g states. These four bands (coming from 2 Cr atoms in the unit cell) are narrow, lie almost completely above the Fermi energy, and hybridize with the graphene Dirac cones in the majority spin channel close to the Dirac point. In contrast, the minority spin Dirac cone remains intact (see cartoon in (4)(b)). Therefore, for one spin channel the Dirac electrons barely notice the presence of the CrI_3 , for the other spin channel, there is a strong hybridization with a narrow band.

The bands structure of the CrI_3 /graphene bilayer/ CrI_3 are shown in figure (3), both for the FM (left) and AF (right) configurations. Both of them show the graphene

bilayer bands and the e_g bands. For the FM case, the shape of the graphene bilayer bands is preserved in one spin channel (the minority spin), but a strong hybridization opens up a gap in the majority spin channel, slightly above the Fermi energy, which lies below the Dirac point. For the AF configuration, both spin channels of the graphene bilayer become hybridized with the narrow e_g bands of CrI_3 . So, from that point of view alone, we expect that the in-plane conductance is much larger in the FM alignment than the AF one.

We now turn our attention to the states around the Dirac energy, where the conduction and valence parabolic bands of freestanding graphene bilayer meet. For the AF configuration, a band-gap splits the electron and hole parabolic of graphene bilayer (see inset of Fig. (4d)), with a gap of 7 meV. For the FM configuration, there is a spin splitting of the bands near the Dirac point, whose magnitude is, interestingly, the same, than the AF gap. So, in that regard, the DFT results for the bilayer graphene placed between two CrI_3 layers are in line with the toy model. However, there is electron transfer from graphene to CrI_3 , so that the Fermi energy does not lie at the Dirac point. It must be noticed that, even if there is charge transfer, we expect a very small in-plane conductance in the CrI_3 , on account of the very small dispersion of the occupied states.

Thus, our DFT calculations strongly suggest that a graphene *bilayer* encapsulated between two layers of CrI_3 will present a strong spin-valve effect, with the FM alignment having a larger in-plane conductance, on account of the fact that bands in one spin-channel are decoupled from the non-dispersive CrI_3 bands, in contrast with the AF, where both spin channels are hybridized. Interestingly, the same mechanism should also apply for the graphene *monolayer*. In addition, for the graphene bilayer, application of a gate voltage could set the Fermi energy at the Dirac point, resulting in a conductor to insulator transition driven by the alignment of the magnetizations.

The control of the relative orientation of the magnetization of the layers could be done by application of a magnetic field, provided that two conditions are met. First, the interlayer coupling should be smaller than the Zeeman coupling. Interlayer coupling of CrI_3 bilayers, without graphene in the middle, meets this demand. The presence of the graphene bilayer should significantly reduce the interlayer coupling. Accordingly, our DFT calculations yield $J < 10\mu\text{eV}$ per unit cell. Second, the switching field of top and bottom layers should be different. A very natural way to achieve that is to pin the magnetization of the bottom layer. This could be done, for instance, using a bilayer of CrI_3 for which antiferromagnetic interlayer coupling has been reported [11, 12, 15–17]

The concept of Van der Waals spin valve goes beyond the case of the graphene bilayer. For instance, the tunable spin proximity effect can drive a metal insulator

transition in a graphene monolayer in the Quantum Hall regime. At half filling, high quality graphene quantum Hall bars are often insulating. Application of a strong in-plane magnetic field can induce a Quantum Hall ferromagnet that has a finite edge conductance [30, 39]. In a spin valve, such transition could be promoted by spin proximity effect, rather than Zeeman interaction. Another possibility are Van der Waals spin valves with a superconducting middle layer, such as NbSe_2 . In the FM state, spin proximity effect can kill superconductivity, that would only survive in the AF state. Such a transition has been observed in superconducting thin films sandwiched between bulk ferromagnetic insulators [40]. The concept of Van der Waals spin valve can be extended to the control of optical properties. For instance, spin proximity might control whether dark or bright excitons of the middle layer are the ground state of the 2D semiconductor.

In conclusion, we have proposed a new type of spin valve where a non-magnetic 2D crystal is sandwiched between two ferromagnetic insulators and its in-plane conductance is controlled by spin proximity effect. We hope that our work will motivate the experimental exploration of Van der Waals current in plane spin valves, including the of other materials in the non-magnetic layers, such as superconductors, as well as other magnetic layers, such as bulk ferromagnets, for which the spin valve effect proposed here should also work.

We acknowledge J. L. Lado for fruitful discussions and technical assistance in the calculations. We acknowledge financial support from FEDER project NORTE-01-0145-FEDER-000019, the Marie Curie Nano TRAIN for Growth Cofund program at INL and FCT for the P2020-PTDC/FIS-NAN/3668/2014 project. We acknowledge Efrén Navarro-Morata for fruitful discussions.

-
- [1] M. N. Baibich, J. M. Broto, A. Fert, F. N. Van Dau, F. Petroff, P. Etienne, G. Creuzet, A. Friederich, and J. Chazelas, *Physical Review Letters* **61**, 2472 (1988).
 - [2] G. Binasch, P. Grünberg, F. Saurenbach, and W. Zinn, *Physical Review B* **39**, 4828 (1989).
 - [3] M. Julliere, *Physics Letters A* **54**, 225 (1975).
 - [4] J. S. Moodera, L. R. Kinder, T. M. Wong, and R. Meserve, *Physical Review Letters* **74**, 3273 (1995).
 - [5] B. Dieny, V. S. Speriosu, S. Metin, S. S. Parkin, B. A. Gurney, P. Baumgart, and D. R. Wilhoit, *Journal of Applied Physics* **69**, 4774 (1991).
 - [6] A. K. Geim and I. V. Grigorieva, *Nature* **499**, 419 (2013).
 - [7] K. Novoselov, A. Mishchenko, A. Carvalho, and A. C. Neto, *Science* **353**, aac9439 (2016).
 - [8] X. Wang, K. Du, Y. Y. F. Liu, P. Hu, J. Zhang, Q. Zhang, M. H. S. Owen, X. Lu, C. K. Gan, P. Sengupta, et al., *2D Materials* **3**, 031009 (2016).
 - [9] J.-U. Lee, S. Lee, J. H. Ryoo, S. Kang, T. Y. Kim, P. Kim, C.-H. Park, J.-G. Park, and H. Cheong, *Nano*

- Letters **16**, 7433 (2016).
- [10] C. Gong, L. Li, Z. Li, H. Ji, A. Stern, Y. Xia, T. Cao, W. Bao, C. Wang, Y. Wang, et al., *Nature* **546**, 265 (2017), ISSN 0028-0836.
 - [11] B. Huang, G. Clark, E. Navarro-Moratalla, D. R. Klein, R. Cheng, K. L. Seyler, D. Zhong, E. Schmidgall, M. A. McGuire, D. H. Cobden, et al., *Nature* **546**, 270 (2017).
 - [12] D. R. Klein, D. MacNeill, J. L. Lado, D. Soriano, E. Navarro-Moratalla, K. Watanabe, T. Taniguchi, S. Manni, P. Canfield, J. Fernández-Rossier, et al., *arXiv preprint arXiv:1801.10075* (2018).
 - [13] T. Song, X. Cai, M. W.-Y. Tu, X. Zhang, B. Huang, N. P. Wilson, K. L. Seyler, L. Zhu, T. Taniguchi, K. Watanabe, et al., *arXiv preprint arXiv:1801.08679* (2018).
 - [14] Z. Wang, I. Gutiérrez-Lezama, N. Ubrig, M. Kroner, T. Taniguchi, K. Watanabe, A. Imamoğlu, E. Giannini, and A. F. Morpurgo, *arXiv preprint arXiv:1801.08188* (2018).
 - [15] S. Jiang, J. Shan, and K. F. Mak, *Nature materials* (2018).
 - [16] B. Huang, G. Clark, D. R. Klein, D. MacNeill, E. Navarro-Moratalla, K. L. Seyler, N. Wilson, M. A. McGuire, D. H. Cobden, D. Xiao, et al., *arXiv:1802.06979v2 [cond-mat.mes-hall]* (2018).
 - [17] S. Jiang, L. Li, Z. Wang, K. F. Mak, and J. Shan, *arXiv:1802.07355v1* (2018).
 - [18] N. Tombros, C. Jozsa, M. Popinciuc, H. T. Jonkman, and B. J. Van Wees, *Nature* **448**, 571 (2007).
 - [19] W. Han, R. K. Kawakami, M. Gmitra, and J. Fabian, *Nature nanotechnology* **9**, 794 (2014).
 - [20] G.-X. Miao, M. Müller, and J. S. Moodera, *Phys. Rev. Lett.* **102**, 076601 (2009).
 - [21] F. Guinea, A. C. Neto, and N. Peres, *Physical Review B* **73**, 245426 (2006).
 - [22] V. T. Phong, N. R. Walet, and F. Guinea, *2D Materials* **5**, 014004 (2017).
 - [23] H. Yang, A. Hallal, D. Terrade, X. Waintal, S. Roche, and M. Chshiev, *Physical Review Letters* **110**, 046603 (2013).
 - [24] A. Hallal, F. Ibrahim, H. Yang, S. Roche, and M. Chshiev, *2D Materials* **4**, 025074 (2017).
 - [25] T. Ohta, A. Bostwick, T. Seyller, K. Horn, and E. Rotenberg, *Science* **313**, 951 (2006).
 - [26] E. McCann, *Phys. Rev. B* **74**, 161403 (2006).
 - [27] J. Fernández-Rossier, *Physical Review B* **77**, 075430 (2008).
 - [28] I. Martin, Y. M. Blanter, and A. Morpurgo, *Physical Review Letters* **100**, 036804 (2008).
 - [29] P. San-Jose, E. Prada, E. McCann, and H. Schomerus, *Physical Review Letters* **102**, 247204 (2009).
 - [30] J. L. Lado, N. García-Martínez, and J. Fernández-Rossier, *Synthetic Metals* **210**, 56 (2015).
 - [31] D. Zhong, K. L. Seyler, X. Linpeng, R. Cheng, N. Sivadas, B. Huang, E. Schmidgall, T. Taniguchi, K. Watanabe, M. A. McGuire, et al., *Science Advances* **3**, e1603113 (2017).
 - [32] P. Giannozzi, S. Baroni, N. Bonini, M. Calandra, R. Car, C. Cavazzoni, D. Ceresoli, G. L. Chiarotti, M. Cococcioni, I. Dabo, et al., *J. Phys.: Condens. Mat.* **21**, 395502 (2009).
 - [33] J. P. Perdew, M. Ernzerhof, and K. Burke, *J. Chem. Phys.* **105**, 9982 (1996).
 - [34] P. E. Blöchl, *Phys. Rev. B* **50**, 17953 (1994).
 - [35] E. Kucukbenli, M. Monni, B. Adetunji, X. Ge, G. Adebayo, N. Marzari, S. De Gironcoli, and A. D. Corso, *arXiv preprint arXiv:1404.3015* (2014).
 - [36] S. Grimme, *J. Comput. Chem.* **27**, 1787 (2006).
 - [37] J. L. Lado and J. Fernández-Rossier, *2D Materials* **4**, 035002 (2017).
 - [38] J. Zhang, B. Zhao, T. Zhou, Y. Xue, C. Ma, and Z. Yang, *arXiv preprint arXiv:1710.06324* (2017).
 - [39] A. Young, J. Sanchez-Yamagishi, B. Hunt, S. Choi, K. Watanabe, T. Taniguchi, R. Ashoori, and P. Jarillo-Herrero, *Nature* **505**, 528 (2014).
 - [40] B. Li, N. Roschewsky, B. A. Assaf, M. Eich, M. Epstein-Martin, D. Heiman, M. Münzenberg, and J. S. Moodera, *Physical Review Letters* **110**, 097001 (2013).